TECHNICAL MEMORANDUMS

NATIONAL ADVISORY COMMITTEE FOR AERONAUTICS

No. 630

THE STEADY SPIN

By Richard Fuchs and Wilhelm Schmidt

Luftfahrtforschung
Vol. III, No. 1, February 27, 1929
Verlag von R. Oldenbourg, München und Berlin

Washington
July, 1931

NATIONAL ADVISORY COMMITTEE FOR AERONAUTICS

TECHNICAL MEMORANDUM NO. 630

THE STEADY SPIN*

By Richard Fuchs and Wilhelm Schmidt

N o t a t i o n

Space axes:

η = space vertical,

ξ = space horizontal, here tangent to a circular cylinder with axis η,

ζ = space horizontal, perpendicular to η and ξ.

Air axes:

x = path axis,

z = space horizontal, perpendicular to x,

y = axis perpendicular to x and z.

Body axes:

$\underline{x}$ = longitudinal axis,

$\underline{y}$ = normal axis,

$\underline{z}$ = lateral axis,

g = acceleration of gravity (m/s^2),

γ = air density (kg/m^3),

$\frac{\gamma}{2g} = \frac{1}{20}$ in this report,

$q = \frac{\gamma}{2g} v^2$ dynamic pressure (kg/m^2).

---

*"Stationärer Trudelflug." From Luftfahrtforschung, Vol. III, No. 1, February 27, 1929, published by R. Oldenbourg, Munich and Berlin, pp. 1-18.

The following data apply to Junkers A 35 low-wing monoplane:

G = 1600 kg, gross weight,

F = 29.76 m^2, wing area,

b = 15.94 m, span,

$t = \frac{F}{b} = 1.87$ m, mean chord,

t_x = wing chord (m),

t_1 = 2.20 m, chord at fuselage,

t_2 = 1.60 m, chord at wing tip,

$\underline{z}$ (m) = distance of wing component $t_x\, d\underline{z}$ from the center of gravity of the airplane S,

h = 0.42 m, center of gravity from wing chord in plane of symmetry,

r = 0.80 m, center of gravity from leading edge,

$J_{\underline{x}}$ = 300 mkgs^2 inertia moment about longitudinal axis,

$J_{\underline{y}}$ = 550 mkgs^2 inertia moment about normal axis,

$J_{\underline{z}}$ = 290 mkgs^2 inertia moment about lateral axis,

φ (deg.) = gliding angle,

ω = rate of rotation about space vertical η (1/s),

$$\left.\begin{aligned}
\omega_x &= \omega \sin\varphi, \\
\omega_y &= \omega \cos\varphi, \\
\omega_{\underline{x}} &= \omega(\cos\varphi \cos\mu \sin\alpha + \sin\varphi \cos\alpha) \\
\omega_{\underline{y}} &= \omega(\cos\varphi \cos\mu \cos\alpha - \sin\varphi \sin\alpha) \\
\omega_{\underline{z}} &= -\,\omega \cos\varphi \sin\mu \\
\omega_{\underline{y}_1} &= \omega \cos\varphi \cos\mu
\end{aligned}\right\} (1/s)$$

All rotations are positive when clockwise as seen in positive direction of rotational axes.

v (m/s) = path velocity,

$\Delta v = \Omega_{\underline{y}_1}\, \underline{z}$ (m/s) change in path velocity v due to rotation $\Omega_{\underline{y}_1}$,

$\rho = \frac{v \cos\varphi}{\omega}$ (m) radius of helix,

α(deg.) = angle of attack
μ(deg.) = angle of bank
as defined in Figure 1

τ(deg.) = angle of yaw, formed by axes $\underline{x}$ and $\underline{z}$ after rotating about normal axis $\underline{y}$,

$\Delta\alpha = 57.3 \arctan \frac{\Omega_x z}{v}$ (deg.) change in α due to rotation Ω_x.

A (kg), $c_a = \frac{A}{qF}$ lift; in direction of lift axis $\underline{y}_1$,

W (kg), $c_w = \frac{W}{qF}$ drag; in opposite direction to path axis x,

Q (kg), $c_Q = \frac{Q}{qF}$ cross wind force; perpendicular to lift and drag,

N (kg), $c_n = \frac{N}{qF} = c_a \cos\alpha + c_w \sin\alpha$ normal force; in direction of normal axis $\underline{y}$,

T (kg), $c_t = \frac{T}{qF} = c_w \cos\alpha - c_a \sin\alpha$ tangential force; opposite in direction to longitudinal axis $\underline{x}$,

M_{L_o} (mkg), $c_{m_o} = \frac{M_{L_o}}{qFt}$ aerodynamic moment about leading edge,

M_L (mkg), $c_m = \frac{M_L}{qFt}$

$\underline{M}_L = \frac{M_L}{\frac{G}{g} v^2}$

aerodynamic moment about lateral axis $\underline{z}$,

M_H (mkg), $\underline{M}_H = \frac{M_H}{\frac{G}{g} v^2}$ elevator moment,

M_K (mkg), $\underline{M}_K = \frac{M_K}{\frac{G}{g} v^2}$ gyroscopic moment about the lateral axis $\underline{z}$,

K_L (mkg), $\underline{K}_L = \frac{K_L}{qFb}$ aerodynamic moment about longitudinal axis $\underline{x}$,

K_F (mkg), $\underline{K}_F = \frac{K_F}{qFb}$, $\underline{K}_F' = \frac{K_F}{\frac{G}{g} v^2}$ aerodynamic moment of wing about longitudinal axis $\underline{x}$,

K_Q (mkg), $\underline{K}_Q = \frac{K_Q}{qFb}$ aileron moment about longitudinal axis $\underline{x}$,

K_K (mkg), $\underline{K}_K = \frac{K_K}{\frac{G}{g} v^2}$ gyroscopic moment about longitudinal axis $\underline{x}$,

L_L (mkg), $\underline{L}_L = \frac{L_L}{qFb}$ aerodynamic moment about normal axis $\underline{y}$,

L_F (mkg), $\underline{L}_F = \frac{L_F}{qFb}$ aerodynamic moment of wing about normal axis $\underline{y}$,

L_S (mkg), $\underline{L}_S = \frac{L_S}{qFb}$ rudder moment about normal axis $\underline{y}$,

L_K (mkg), $\underline{L}_K = \frac{L_K}{qFb}$ gyroscopic moment about normal axis $\underline{y}$.

All moments, opposite in direction to the corresponding positive rotations, are positive:

β_H(deg.) elevator setting, < 0 displacement upward,
> 0 " downward.

β_H(deg.) rudder displacement,

β_H(deg.) aileron " .

All control movements producing positive moments are positive.

This report attempts a comprehensive survey of the subject of spinning, and constitutes an extension and supplement to Fuchs and Hopf's "Aerodynamik," chapter IV.

Several British reports (references 4 and 5) carry the notation that the angle of yaw is relatively small in spinning and rarely exceeds 20°. The English have established the effect of side slip for the most necessary data in the wind tunnel at angles of side slip $\tau < \sim 20^\circ$.

It is readily seen from Figures 5 and 6 (reference 6) that the change in lift and drag with side slip amounts, at the most, to 10% of the corresponding values with no side slip so long as the yaw does not exceed 20°.

In Figure 7 (reference 6) cross-wind force c_Q, perpendicular to lift and drag at $\tau = 20^\circ$ with side slip has attained about 10% of lift with no side slip.

The change of aerodynamic moment about the lateral axis, due to side slip becomes significant, according to Figure 8 (reference 7), even though $\tau < 20^\circ$.

Figures 9 and 10 (references 4 and 8) disclose that, as a result of a rotation around the path axis, the rolling and yawing moments are materially changed, as in curves a_1 with no side slip or aileron displacement, in curves a_2 with aileron displacement, and especially in curves b with side slip.

It is seen, for example, with respect to the moments about the longitudinal axis for $\alpha = 25^\circ$ that the effect of a side slip at $\tau = 9.5^\circ$ is equivalent to an aileron deflection $\beta_Q = 5^\circ$.

Thus, the ensuing investigation proceeds from the following evidence:

So long as $\tau < 20^\circ$, the changes in lift and drag do not exceed 10% with no side slip; the cross-wind force amounts, at the highest, to 10% of the lift. Hence the computed v, μ and ω values for $\tau = 0^\circ$, as based upon c_a, c_w and c_Q, will undergo no substantial change for any angle of yaw below 20°.

But the moments about the body axes undergo marked changes with side slip. On the other hand, the aerodynamic moment about the longitudinal axis can be produced by a suitably chosen aileron displacement, according to Figure 9, and the same applies to the moments about the normal and the lateral axes, as the corresponding elevator, rudder, or aileron displacements are introduced.

When we bear in mind the fact that side slip and the corresponding control movements are identical in effect, the balance of the moments about the body axes <u>with side slip</u> is all but revertible to an equilibrium by corresponding control movements but with <u>no side slip</u>.

Thus it becomes readily apparent that a study at $\tau = 0^\circ$ is not materially altered when it includes the changes in aerodynamic forces and moments resulting from side slip at $\tau < 20^\circ$.

For this reason we repeated our investigation for the case of $\tau = 0^\circ$, but confined ourselves for the most part to the steady spin.

Calculations on unsteady spinning are made only occasionally, where it pertains to a numerical integration of the differential equations set up for the equilibrium of all forces and moments acting on the airplane, and then only to several short equations in order to clarify the problem of getting out of a spin.

The steady spin without side slip postulates:

Equilibrium of forces in direction of the air axes -

Path axis x: $0 = G \sin\varphi - c_w\, q\, F$ (1)

Lift axis $\underline{y}_1$: $0 = \frac{G}{g}\, v\, \omega_y \sin\mu - G \cos\varphi \cos\mu + c_a\, q\, F$ (2)

Axis $\perp$ x and $\underline{y}_1$: $0 = \frac{G}{g}\, v\, \omega_y \cos\mu + G \cos\varphi \sin\mu$ (3)

Equilibrium of moments about the body axes:

Longitudinal axis $\underline{x}$: $-(J_{\underline{y}} - J_{\underline{z}})\, \omega_{\underline{y}}\, \omega_{\underline{z}} = -K$ (4)

Normal axis $\underline{y}$: $-(J_{\underline{z}} - J_{\underline{x}})\, \omega_{\underline{z}}\, \omega_{\underline{x}} = -L$ (5)

Lateral axis $\underline{z}$: $-(J_{\underline{x}} - J_{\underline{y}})\, \omega_{\underline{x}}\, \omega_{\underline{y}} = -M$ (6)

The above six equations embody the five variables:

α, μ, v, φ and ω, and reveal in conjunction with $\tau = 0$, the position of the airplane completely.

The resolution of equations (1) to (3) yields in dependence of α and φ, the other three variables μ, v, and ω, for which all forces acting on the airplane are in balance.

Applying these values to each one of equations (4), (5), and (6) results in α and φ values, at which, by equilibrium of all forces acting on the airplane, the moments about the respective axis are also in equilibrium.

If these values of φ and α are plotted as curves of $\varphi = f(\alpha)$, three such curves are obtained corresponding to the three equations (4) to (6). From each of these three curves those values of α and φ are found at possible intersection points for which the simultaneous equilibrium of all the forces and all the moments is satisfied, and for which, therefore, the steady spin is possible.

Our investigations centered around a Junkers A 35 low-wing monoplane with the latest test data on c_a, c_w, and c_m, and for angles of attack up to $\alpha = 90^\circ$. Unfortunately they were limited to a stationary model without aileron or rudder displacement and for certain elevator settings within $\alpha = 0$ to $\alpha = 20^\circ$.

The change in lift and drag within this range is slight with elevator displacement, as Figure 14 shows. In addition, other pertinent data disclosed the aileron and rudder movements to be practically without effect on the aerodynamic forces, and notably on the aerodynamic moment about the lateral axis, so that it is justifiable to assume c_a and c_w, especially at higher α, as constant for any control movement, and c_Q as evanescently small at zero yaw.

According to the British reports the principal changes in forces and moments about the lateral axis, effected by rotation ω occur in the lift and in the drag, as shown in Figures 11 and 12 (reference 4). Even for values of $\frac{b\omega_x}{2\,v} = 0.2$ to 0.3, encountered perhaps in a steep spin at relatively small α, the change in c_a

and c_w amounts to about 10% of the values measured on the quietly suspended model. So lift and drag may be considered approximately constant for the rotations in question.

Figure 13 (reference 7) reveals the relatively slight change in moment about the lateral axis when rotated about the path axis at large angles of attack; at small α the change is more pronounced and is equivalent to a small elevator displacement. Nevertheless, we consider c_m as being about constant for any value of $\frac{b\omega_x}{2\,v}$, so that the aerodynamic forces as well as the aerodynamic moments about the lateral axis may be assumed approximately constant, for all rotations ω under consideration.

As regards the magnitude of the control moments, we were compelled to introduce them for large values of α without data on the corresponding control displacements, and to refer for small α in part to measured elevator setting, and in part to estimated aileron or rudder displacement.

The wing moments K_F and L_F about the longitudinal and the normal axis were not measured, but were accurately estimated by integration and by means of curves c_n and c_t with respect to α. The inertia moments were defined by calculation as usual.

Equilibrium of Forces and Moments in Steady Spin with no Side Slip

Equations (1) to (3) yield the values μ, v and ω dependent on α and φ for steady spin as

$$\mu = -\,57.3 \text{ arc tan}\left(\frac{v\,\omega}{g}\right) \tag{7}$$

$$v = \sqrt{-\,\frac{G\;2\;g}{F\;\gamma}\;\frac{\sin\varphi}{c_w}} \tag{8}$$

$$\omega = \sqrt{\frac{F^2\;\gamma^2}{4\;G^2}\;\frac{{c_a}^2\;v^2}{\cos^2\varphi} - \frac{g^2}{v^2}} \tag{9}$$

The c_a and c_w values applying to the airplane were taken from Figure 14, while Figure 15 shows

$$v = \sqrt{-1075 \frac{\sin \varphi}{c_w}}$$

plotted against α and φ. The path velocity rises with increasing angle of climb and drops as the drag increases.

Figure 16 manifests

$$\omega = \sqrt{0.000083 \frac{{c_a}^2 \ v^2}{\cos^2 \varphi} - \frac{96}{v^2}}$$

relative to α and φ. The rate of rotation increases enormously by rising angle of climb and disappears for level flight. For the latter the modified equations (1a) to (3a) are valid:

$$0 = - G \sin \varphi - c_w \, q \, F \tag{1a}$$

$$0 = - G \cos \varphi \cos \mu + c_a \, q \, F \tag{2a}$$

$$0 = G \cos \varphi \sin \mu \tag{3a}$$

as a consequence of which $\mu = 0$ and $\tan \varphi = - \frac{c_w}{c_a}$.

Figure 17 exhibits $\tan \varphi = - \frac{c_w}{c_a}$, as well as the corresponding values of φ referable to α, so that α may be read from Figure 17 for certain values of φ where $\omega = 0$.

The introduction of constant values ω other than zero into equations (1) to (3) yields $\varphi\,(\omega = \text{constant})$ (fig. 17) with respect to α, which were taken from curves ω plotted against α and φ in Figure 16.

Figure 18 shows $\mu = - \text{arc tan} \left(\frac{v\omega}{g}\right)$ with respect to α and φ. Even in a flat glide the angle of bank becomes very pronounced at the usual angles of attack, while an airplane already inclines quite steeply in ordinary curve flight. When $\omega = 0$, μ disappears.

To compute the gyroscopic moments the rate of rotations $\omega_{\underline{x}}$, $\omega_{\underline{y}}$ and $\omega_{\underline{z}}$ are necessary.

Conformably to Figure 16, ω does not become appreciable at small gliding angles; but when these angles become large, μ becomes large also, according to Figure 18, in which case

$$\omega_{\underline{x}} \approx - \omega \cos \alpha$$

$$\omega_{\underline{y}} \approx \omega \sin \alpha$$

$$\omega_{\underline{z}} \approx 0,$$

which, geometrically speaking, means:

We can indicate a straight line placed in the symmetrical plane of the aircraft, which passes through its center of gravity, forms angle α with the longitudinal axis and is parallel to that of the space vertical about which rotation ω is set up. The distance of the space vertical from this straight line is

$$\rho = \frac{v \cos \varphi}{\omega}.$$

For the case of $\varphi \to - 90^{\circ}$, we find ω ∞, according to (9) while v (according to (8)) reveals a tendency toward a fixed value, so that distance ρ becomes very minute and rotation ω is almost around the above straight line. Then the greater α becomes the more this straight line is coincident with the normal axis.

In Figure 19 the rate of rotation for $\omega_{\underline{x}}$, $\omega_{\underline{y}}$ and $\omega_{\underline{z}}$ is given for $\varphi = - 85^{\circ}$, -80° and -75°. It will be noted that rate of rotation $\omega_{\underline{z}}$ about the lateral axis is always very low, that rotation $\omega_{\underline{x}}$ about the longitudinal axis predominates at small α, and rotation $\omega_{\underline{y}}$ about the normal axis when α is high.

The equilibrium of the moments

α) about the lateral axis is based upon:

$$(J_{\underline{x}} - J_{\underline{y}})\, \omega_{\underline{x}}\, \omega_{\underline{y}} = M_L$$

negative gyroscopic moment $(- M_{\underline{K}})$ = aerodynamic moment M_L.

With the nondimensional $\underline{M}_K = \frac{M_K}{\frac{G}{g} v^2}$ inserted, we obtain

$$\underline{M}_K = - \frac{(J_{\underline{x}} - J_{\underline{y}})}{\frac{G}{g}} \frac{\omega^2}{v^2} \begin{array}{l}(\cos \varphi \cos \mu \sin \alpha + \sin \varphi \cos \alpha \\ (\cos \varphi \cos \mu \cos \alpha - \sin \varphi \sin \alpha),\end{array}$$

which may be seen on Figure 20 in relation to α and φ. The gyroscopic moments do not appear until the gliding angles are very high, and become very pronounced when $\varphi > - 85°$.

The aerodynamic moment, defined as $\underline{M}_{L_o} = c_{m_o}\ q\ F\ t$ on the leading edge of the stationary model in the wind tunnel and reproduced in Figure 14 with respect to α was replotted for moment M_L about the lateral axis and expressed in the same nondimensional form as $\underline{M}_K$, that is, we substituted

$$\underline{M}_L = \frac{M_L}{\frac{G}{g} v^2} = 0.017\ c_m \quad \text{for} \quad c_m = \frac{M_L}{qFt}$$

Figure 20 shows $\underline{M}_L$ plotted against α for various additional elevator moments

$$\underline{M}_H = \frac{M_H}{\frac{G}{g} v^2}$$

constant at any α, to which at small α a given elevator setting β_H corresponds. It is noted that curve $(- \underline{M}_K)$, referred to α and φ, and curve $\underline{M}_L$ referred to α intersect in several points for which $(M_K) = M_L$; that is, where the moments about the lateral axis are in balance.

β) The equilibrium of the moments about the longitudinal axis is expressed by

$$(J_{\underline{y}} - J_{\underline{z}})\ \omega_{\underline{y}}\ \omega_{\underline{z}} = K_L$$

negative gyroscopic moment $(- K_K)$ = aerodynamic moment K_L.

The rotation ω_x about the path axis induces wing moments about the longitudinal axis exceeding by far any eventual aileron moment K_Q. A damping moment of the vertical tail group as occurs because of rotation ω_x about the longitudinal axis, may be disregarded.

The integration estimates the aerodynamic moments of the wings at

$$K_F = \int_{z=-\frac{b}{2}}^{+\frac{b}{2}} c_n\,(\alpha + \Delta\alpha,\ v + \Delta v)\ \frac{\gamma}{2g}\left(\frac{v + \Delta v}{\cos \Delta\alpha}\right)^2 t_x\ z\ d\ z$$

In particular, $c_n\ (\alpha + \Delta\alpha,\ v + \Delta v)$ here signifies that c_n is affected by α and by its effected change through $\Delta\alpha = 57.3 \text{ arc tan } \frac{\omega_x\ z}{v + \Delta v}$ because of rotation ω_x, further by speed v and its change through $\Delta v = \omega_{y_1}\ z$ because of rotation ω_{y_1}.

The integral was graphically determined against α and φ so as to include any value of $\frac{b\ \omega_x}{2\ v}$.

To give the reader a picture of the method employed, we include Figure 21 as typifying the distribution of the normal force over the wing; $c_n\ \left(\frac{v + \Delta v}{\cos \Delta\alpha}\right)^2\ t_x$ is plotted against wing span z, where the integral evaluates precisely $K_F = 0$. Now it becomes evident that for $\varphi = -80^\circ$ and $\alpha = -27^\circ$, the wing moment about the longitudinal axis is zero notwithstanding the prevalent rotation ω_x.

Figure 22 affords $k_F = \frac{K_F}{qFb}$ against α and φ, and the possibility of positive and negative wing moments. They disappear when $\omega = 0$ (the relevant points may be called outer zero points), the α values pertinent for φ may be taken from the curve of Figure 17. For slow rates of rotations ω_x, where $\Delta\alpha$ too is small, the integral obviously becomes evanescent at values of α for which curve c_n, referred to α in Figure 23, exhibits an extreme value, namely, point G for $\alpha = 14^\circ$ and point H for $\alpha = 32^\circ$. Moreover, it is positive or negative according to whether $\frac{dc_n}{d\alpha}$ is $>$ or $<$ 0.

In keeping with this, small φ values, for which, consistently with Figure 16, the rate of rotation ω as well as $\Delta\alpha$ are small, have, apart from the two outer-also one or two inner points G and H; in addition, for $\alpha < 14^\circ$ and $\alpha > 32^\circ$, where $\frac{dc_n}{d\alpha} > 0$, only negative wing moments, and for $\alpha > 14^\circ$ and $\alpha < 32^\circ$, where $\frac{dc_n}{d\alpha} > 0$, only positive wing moments occur. As φ and thereby $\Delta\alpha$ become larger, the positive moments become more and more evanescent, the zero points G and H continue to come closer together and to assume still greater values of α, until only negative moments appear.

With the gyroscopic moment K_K expressed nondimensionally

$$\underline{K}_K = \frac{K_K}{\frac{G}{g} v^2},$$

we have:

$$\underline{K}_K = -\frac{(J_y - J_z)}{\frac{G}{g}} \frac{\omega^2}{v^2} (\cos\varphi \cos\mu \cos\alpha - \sin\varphi \sin\alpha) \cos\varphi \sin\mu.$$

In conformity with Figure 19, the gyroscopic moment is dependent on the always small rotation ω_z, hence is itself very small, as indicated on Figure 24, and may be neglected with respect to K_F.

As a result, our assumption is sufficiently precise when it presumes the moments about the longitudinal axis to be almost in balance for those values of α and φ for which the moments of the wings disappear, or in other words, for the zero positions of curve $\underline{K}_F$ with respect to α and φ, at least so long as no aileron displacement occurs.

The insertion of an aileron moment, constant for any α,

$$\underline{K}_Q = \frac{K_Q}{qFb} = \pm\ 0.01$$

rather corresponds at $\alpha = 0^\circ$ to a $\beta_Q = \pm\ 4^\circ$ aileron deflection, but at higher α to a much greater deflection, so the abscissa of the curves must be shifted parallel to itself, upward and downward, respectively.

γ) The moment equilibrium about the normal axis is expressed by equation

$$(J_z - J_x)\,\omega_z\,\omega_x = L_L,$$

negative gyroscopic moment $(-L_K)$ = aerodynamic moment L_L.

The rotation ω_x about the path axis induces wing moments, which, aside from a rudder moment and from the far from negligible damping moment of the fuselage and the vertical tail group, such as a rotation ω_y about the normal axis sets up, constitute the principal moments acting about the normal axis.

Evaluated by integration, the wing moments are

$$L_F = \int_{z=-\frac{b}{2}}^{+\frac{b}{2}} c_t\,(\alpha + \Delta\alpha,\ v + \Delta v)\ \frac{\gamma}{2g}\left(\frac{v + \Delta v}{\cos \Delta\alpha}\right)^2 t_x\, z\, d\, z,$$

which, in Figure 25, are plotted with reference to α and φ in the nondimensional form of

$$L_F = \frac{L_F}{qFb}.$$

The outer zero positions are valid for $\omega = 0$, the inner when the integral disappears, i.e., first at small φ and ω for points K and J of curve c_t, as plotted against α in Figure 23, where $\frac{dc_t}{d\alpha} = 0$. The wing moments become positive or negative according to whether $\frac{dc_t}{d\alpha} < \text{or} > 0$.

The zero points K and J tend toward higher α and come closer together as φ increases. At very high α the moments about the normal axis become quite small.

The gyroscopic moment $L_K = -(J_z - J_x)\,\omega_z\,\omega_x$ may be disregarded with respect to L_F.

As a result the moments about the normal axis are practically in balance for those α and φ at which L_F disappears, i.e., for the zero points of the L_F curves referred to α and φ at least as long as there is no rudder displacement, and the damping moments of the fuselage and of the vertical tail surfaces due to rotation ω_y about the normal axis are disregarded for the present owing to the lack of experimental data.

With an added rudder moment, constant for any α, we have:

$$\underline{L}_S = \frac{L_S}{qFb} = \pm 0.01,$$

which at $\alpha = 0^\circ$, is practically equivalent to a $\beta_S = \pm 20^\circ$ rudder displacement, but at higher α to one decidedly higher; thus the abscissa of the curves must be shifted parallel downward and upward, respectively.

The damping moments of the fuselage and of the vertical tail group, induced by rotation ω_y about the normal axis, play a very important part in the moment equilibrium about the normal axis and must not be ignored. If the vertical tail group, and particularly the rear end of the fuselage, present a large area relatively remote from the normal axis, they may in fact become just as high as the wing moments L_F, and even surpass them at large α.

Hitherto our study defined the values for α and φ at which the forces and moments about the three body axes were in equilibrium, as exhibited in Figure 26 for the special case of β_Q and $\beta_S = 0^\circ$ with φ plotted against α, disregarding the damping caused by the fuselage and by the vertical tail unit. Curve a comprises those values of α and φ for which, if $\omega = 0$, all forces acting on the airplane are in equilibrium and, since the moments must also be in equilibrium if the spin is to be steady, where all curves of the moment equilibrium must start on this curve a. The b curves divulge the equilibrium of the moments about the lateral axis with the respective elevator moments.

As long as rotation ω remains small, i.e., for relatively small φ as shown in Figure 17, there are practically no gyroscopic moments (see fig. 20), so that, for a given elevator moment, those about the lateral axis are in equilibrium for those values of α which Figure 20 reveals as zero points on the $\underline{M}_L$ curve referable to α.

Consequently, curve b_1 must begin at point A on curve a and which further belongs to an angle of attack

$\alpha = 12^\circ$. For the coordinates of this point, that is, for $\varphi = -7.5^\circ$ and $\alpha = 12^\circ$, and for these alone, a steady spin is possible without elevator displacement. Points B and C are defined in the same manner.

The greater the gliding angle φ and thereby rate of rotation ω, the greater the gyroscopic moments and the greater the tendency of the intersections of the $\underline{M}_L$ and the $(\underline{M}_K)$ curves toward higher angles of attack (fig. 20), thus deflecting the b curves more and more to the right.

At relatively small α and φ the b curves are quite far apart for different elevator moments, but come quite close to one another when α and φ assume large values.

The d_1 and the e_1 curves pertain to the equilibrium of the moments about the longitudinal and the normal axis, respectively, by zero control displacement.

Now we add an aileron moment, constant for any α, to those about the longitudinal axis of Figure 22, and obtain new zero points on the $\underline{K}_F$ curves with respect to α and φ, whose coordinates are shown in Figure 27 as new curves d with parameter $\underline{K}_Q$.

It is seen that the d curves are far apart while α is relatively small, and continue to approach one another at high α as φ becomes larger.

A similar study reveals the e curves in Figure 28 by rudder moment L_S. At large angles of attack this moment is usually very small, making any equilibrium for α and φ values other than the wing moment impossible, at least so long as the damping moments of the fuselage and the vertical control surfaces are disregarded. These damping moments may become comparatively large, thus making a moment equilibrium possible only for a small angle of attack.

A glance at Figure 26 discloses the fact that curves b, d and e, even when disregarding the damping moments of the fuselage and of the vertical tail surfaces, never intersect in one single point if no control movement occurs. The result is that as far as concerns the A 35, a steady spin is impossible without control displacements.

However, it is quite possible to force such an intersection point as, for instance, by a slight negative elevator displacement $\beta_H = -3^\circ$ which yields point E.

Any steady curve flight is possible depending on the chosen control movement - at least, for comparatively low angles of attack. However, at very high angles α, say, near point F, the b, d and e curves most probably never meet in one point; but, since the curves are so close together, and there prevails at least an almost perfect balance of forces and moments, we shall designate such as "approaching steady" spin.

When the possible curve flight is very steep and the respective angle of attack is above that for maximum lift, we ordinarily speak of "spinning" and we distinguish the "steep" from the "flat" spin, according to whether the angle of attack is near that for maximum lift or very large.

The tendency of an airplane to spin depends on the mass distribution, the shape of the wing structure, the position of the center of gravity, the area of the exposed fuselage and the vertical tail group and its distance from the normal axis.

Hopf (reference 2) has already pointed out (see reference 1, chapter IV) that the mass distribution predicts the magnitude of the gyroscopic moments $(J_x - J_y)$ $\omega_x\ \omega_y$ and thereby the moment equilibrium about the lateral axis.

Assuming the mass distribution so changed that factor $(J_x - J_y)$, and thereby the gyroscopic moments, increase to double and to half the value, yields the c_1 and c_2 curves in Figure 26.

The b and c curves bespeak a less pronounced deflection as $(J_x - J_y)$ decreases. If it were possible to so design an airplane that $J_x = J_y$, it would theoretically preclude the inception of any gyroscopic moment about the lateral axis; the b and c curves would run parallel to the ordinate axis. For very small $J_x - J_y$ the b curves would not deflect to the right until very high gliding angles were reached but would then deflect that much sharper, and become $\varphi \approx -90^\circ$

for higher α, thus moving a considerable distance away from the other d and e curves.

The result would be that at small $J_x - J_y$ curvilinear flight would be impossible for angles of attack above those attainable in level flight but not as yet belonging to a flat spin.

Thus it becomes apparent that spinning may be prevented more or less completely, at least for an average range of α, by judicious mass distribution.

We have seen that a rotation about the path, the longitudinal, or the normal axis may engender positive and negative wing moments. It is not easily conceived how the moments about the normal axis with respect to those about the longitudinal axis can be disregarded, as is done quite frequently. For a glance at Figure 25 reveals them of almost the same magnitude as the positive moments about the longitudinal axis in Figure 22.

However, we confine our study to the moments about the longitudinal axis and merely add that the same is equally applicable to the normal axis.

Figure 22 unfolds zero points on the $\underline{K}_F$ curves plotted against α and φ, for angles of attack beyond those of maximum lift and for whose coordinates the moments about the longitudinal axis are in equilibrium. Now compare the d_1 curve of Figure 26 for the case of zero aileron moments:

a, equilibrium of forces in straight glide
" " " and moments
b_1, about lateral axis
b_2, " " "
b_3, " " "
c_1, " " "
c_2, " " "
d_1, " longitudinal axis
e_1, " normal axis

$\underline{M}_H = 0$

$\underline{M}_H = -0.0011$ (displacement upward)

$\underline{M}_H \cong +0.0010$ (" downward)

$\underline{M}_H = 0$ and double gyroscopic moment,

$\underline{M}_H = 0$ and half gyroscopic moment,

$\underline{M}_H = 0$,

$\underline{M}_H = 0$.

The possibility of spinning, i.e., of a more or less complete balance of forces and moments in stalled steep curve flight depends on the existence of one intersection point each from the three curves b, d and e by corresponding control moment as parameter. Because this is impossible when, for example, curve d is not present, it is merely necessary to prevent the appearance of the inner zero points on curve $\underline{K}_F$ with respect to α and φ, even for any possible aileron moment to make spinning absolutely impossible.

We have seen that the wing moments about the longitudinal axis are dependent only on the shape of curve c_n with respect to angle of attack, and that for small ω_x these moments are negative or positive according to whether $\frac{dc_n}{d\alpha} >$ or < 0. Only negative moments prevail when the c_n curve, valid for each wing section parallel to the plane of symmetry, continues to rise with increasing α. This depends on the shape of the wing, and thus constitutes a second means for limiting the chances of spinning.

Even if it should prove impossible to completely avoid a $c_{n_{max}}$ of the wings alone, it should at least be endeavored to have this occur at the highest possible α and yet not too high, in order to prevent as much as possible a drop in the c_n curve when α assumes large values.

Another successful method for combating the possibility of spinning lies in the constructive development of the airplane with respect to the position of the center of gravity, which in the A 35 is 0.36t aft of the leading edge, that is, relatively far back. The result is that in level flight, for instance, even by zero elevator displacement, the airplane does not attain equilibrium before fairly large angles of attack have been reached and the airplane can be stalled considerably.

Consequently the b curves are easily made to intersect curves d and e in one point.

Shifting the center of gravity extremely far forward renders this stall very difficult to reach. As last and final antispinning method expounded in this study, we mention the shape of the fuselage and of the vertical tail group. With the sides of the rear fuselage, and the area of fin and rudder as large as possible, relatively large damping moments are invited, which, in particular, may make a flat spin very improbable.

Autorotation

In view of the fact that in a spin the rate of rotation ω_{y_1} with respect to ω_x is very low, the resulting aerodynamic moments will always show satisfactory agreement with practical experience when the measurements are made as follows.

The model is mounted on an axis AB passing through its center of gravity and placed in its plane of symmetry so that any angle of attack may be obtained and the moments about the body axes can be measured direct.

Then axis AB is suspended in the wind tunnel so as to be always in the direction of the air flow and so that the model is actually able to execute the desired rotation ω_x. Since we did not make such measurements on the model of the A 35 we interpreted mathematically the K_F and L_F curves shown on Figures 22, 25, 29 and 30, plotted against α and φ, and against α and $\frac{b\omega_x}{2\,v}$, respectively.

The zero points of these curves reveal those values of α and $\frac{b\omega_x}{2\,v}$ for which the aerodynamic moments about the longitudinal and the normal axis are in equilibrium, whereby the abscissas are shifted parallel to one another for existing aileron and rudder moments - constant over any $\frac{b\omega_x}{2\,v}$.

The $\frac{b\omega_x}{2\,v}$ values thus obtained are shown for moment equilibirum about the longitudinal axis on Figure 31, plotted against angle of attack α.

It discloses, for the case of zero aileron moment, a curve similar to those known from the ordinary autorotation tests. Apparently several equilibrium positions are feasible for one and the same α, which is only attributable to the shape of curve c_n with respect to the angle of attack α of the wings.

As regards the stability of the equilibrium positions of the K_F curves plotted against α and $\frac{b\omega_x}{2\,v}$ in Figure 29, a discussion of equation

$$J_x \frac{d\omega_x}{d\,t} - (J_y - J_z)\,\omega_y\,\omega_z = -\,K_F$$

(equilibrium of moments about longitudinal axis) discloses:

If several equilibrium positions prevail, one must always be stable, the other unstable, according to whether

$$\frac{d\,K_F}{d\left(\frac{b\omega_x}{2\,v}\right)} > \text{or} < 0.$$

Applied to curve $\frac{b\omega_x}{2\,v}$ plotted against α in Figure 31 it postulates:

For small angles of attack up to $\alpha = 14^\circ$ there is but one single position of equilibrium where $\frac{b\omega_x}{2\,v} = 0$; autorotation would not set in.

An angle $\alpha > 14^\circ$ has for a certain α, aside from the equilibrium position

$$\frac{b\omega_x}{2\,v} = 0,$$

still a second which, conformably to the general discussions, is stable, while $\frac{b\omega_x}{2\,v} = 0$ becomes unstable. Here autorotation would set in.

Beginning at $\alpha = 32^\circ$, there are, aside from $\frac{b\omega_x}{2\,v} = 0$ two more equilibrium positions, of which since the topmost is always stable and the positions alternatingly stable or unstable, the lowest $\frac{b\omega_x}{2\,v} = 0$ is stable again.

At $\alpha = 55°$ a special position R (see fig. 29) appears, in which one stable and one unstable position of equilibrium coincide.

A comparison with the c_n curve plotted against α in Figure 23, discloses:

The $\frac{b\,\omega_x}{2\,v} = 0$ values relate to stable equilibrium positions so long as $\frac{dc_n}{d\alpha} > 0$, and to unstable positions when $\frac{dc_n}{d\alpha} < 0$.

G and H on Figure 31, the points of transition from stability to instability and vice versa, correspond to points G and H on Figure 23; that is, to the extreme values of the c_n curves with respect to α, for which $\frac{dc_n}{d\alpha} = 0$.

Hence the important conclusion:

The ranges of α for $\frac{b\,\omega_x}{2\,v} = 0$, stable or unstable, or in other words, where autorotation about the longitudinal axis would or would not occur, can forthwith be read from the c_n curve referable to α. So long as $\frac{dc_n}{d\alpha} > 0$, the equilibrium position $\frac{b\,\omega_x}{2\,v} = 0$ is unstable, i.e., autorotation sets in. But, when $\frac{dc_n}{d\alpha} > 0$, $\frac{b\,\omega_x}{2\,v} = 0$ is stable; autorotation cannot set in.

When we introduce an aileron moment $\underline{K}_Q$, constant for any $\frac{b\,\omega_x}{2\,v}$, the abscissa in Figure 29 must be shifted parallel upward or downward, according to whether $\underline{K}_Q$ is negative or positive. In this manner we obtain the new equilibrium positions shown on Figure 31 against α with $\underline{K}_Q$ as parameter.

A positive aileron moment, that is, one which in ordinary flight would turn the airplane still more in a turn, extends the range of autorotation, while a negative moment decreases it.

Figure 32, taken from a British report (reference 8) reveals similar curves for a biplane. Here, however, it was not, as above, a question of equilibrium of aerodynamic moments about the longitudinal axis, but about the path axis.

Figures 33 and 34 (references 7 and 9), also taken from a British report, apply to the moment equilibrium about path axis x, about which the rotation ω_x occurred.

Wing gap, stagger, decálage and aileron displacement effect in general a change in mutual interference, hence in autorotation.

Increased wing gap, positive stagger, top wing ahead, positive decalage and aileron displacement, which ordinarily would force the airplane out of the curve, are conducive to the diminution of magnitude and range of autorotation.

Effect of elevator displacement in steep and flat spin:

It is generally conceded that any control displacement in a steep spin effects an immediate and powerful disturbance of the prevailing flight attitude, but that all control displacements are obviously ineffective in a flat spin. Pushing the control stick forward is the best means, if any, to recover from the spin. These facts agree very well with our calculations.

For the steep spin curves b, d and e in Figure 26, reveal distinctly expressed intersections which prevail for well-defined control displacements only; the curves for the corresponding control displacements are, moreover, far apart.

In a flat spin the conditions are different. Distinct intersections on the three curves b, d and e are most likely altogether precluded; the curves for all control displacements are very close together.

So in order to presage the manner, and more particularly, the time interval during which the momentarily present flight attitude is changed, we made several calculations on unsteady flight. We limited ourselves to the effect of a positive elevator displacement (pushing); once in a steep, perfectly steady spin, then in a flat, "approaching steady" spin - (E and F on Figure 26).

We defined the two flights as follows:

	α	μ	τ	φ	v	ω	S number of turns	β_H	β_Q	β_S
Steep spin	17.0	-85.4	0	-67.5	61.8	1.96	3.2	-3	0	0
Flat spin	64.0	-84.2	0	-87.0	28.9	3.32	1.9	0	0	0

We started with the differential equations defining the equilibrium of all forces and moments acting on the airplane; then we introduced an additional elevator moment $\underline{M}_H = + 0.0021$, which corresponds to a $\beta_H = + 10^\circ$ elevator displacement at small α. This was used to disturb the "perfect" as well as the "approaching perfect" position of equilibrium in the steady and in the flat spin.

Numerically integrated in 1/20 and 1/10 second intervals, the differential equations revealed the data graphed in Figures 35 to 37.

In a steep spin a push on the control stick effects an instantaneous and powerful change in flight attitude. The angle of attack, in particular, promptly assumes a normal range, and the rate of rotation ω drops very quickly. (Reference 10.)

In a flat spin the effect of "pushing" is altogether different. The gradual and seemingly periodic change in angle of attack is striking. An equally periodic change in all other variables is bound up with it, so that the airplane, if at all able, would assume another and, above all, normal attitude of flight only very slowly. The fact that pilots who went into a flat spin unintentionally were able to get out of it again by alternatingly pushing and pulling in the tempo of the ensuing vibrations, seems to bear out our contention.

C o n c l u s i o n

With the object of further clarifying the problem of spinning, and to supplement and extend the data in Fuchs and Hopf's "Aerodynamik," Chapter IV (reference 1), the equilibrium of the forces and moments acting on an airplane is discussed in the light of the most recent test data. Convinced that in a spin the flight attitude by only small angles of yaw is more or less completely steady, the study is primarily devoted to an investigation of steady spin with no side slip. At small α, wholly arbitrary and perfectly steady spins may be forced, depending on the type of control displacements. But at large α only very steep and only "approaching steady" spins are possible, no matter what the control displacements.

A steep curve flight for which, in addition, the angle of attack exceeds even that for maximum lift, is generally called "spin" and we distinguish the "steep spin" from the "flat spin" according to whether the angle of attack is near to that for maximum lift or very large.

From the designer's point of view, the spinning tendency of an airplane can be materially lowered by:

1) Wing shape: a continuous rise of the c_n curve against α valid for each wing cross section parallel to the symmetrical plane. Even if not altogether unavoidable, the $c_{n_{max}}$ should not occur until very high angles of attack have been reached, and should only be so large that the drop in the c_n curve is as small as possible for high values of α.

2) Mass distribution: inertia moment J_x about the longitudinal axis and inertia moment J_y about the normal axis should be as nearly alike as possible.

3) Position of the center of gravity of the airplane: should be extremely far forward.

4) Correct shape of rear end of fuselage and of vertical tail group: the sides of the fuselage, particularly at the rear end, as well as the area of the vertical tail group should be as large as possible and be exposed to the air stream in all directions.

It is expressly emphasized that these exigencies were set up without regard to any other flight characteristic, and merely from the point of view of preventing as far as possible, the entry into a spin.

A study of the effect of control displacements in the discussed spinning attitudes reveals that the steep spin, in contrast to the flat - and I think most exhibition flights belong in this class - can be reverted to normal flight in very short time and is, for that reason, not dangerous.

References and Bibliography

Reference 1. Fuchs and Hopf: Aerodynamik, published by R. C. Schmidt & Co., Berlin W 62, 1922.

Reference 2. Hopf, L.: Flug und Trudelkurven. Zeitschrift für Flugtechnik und Motorluftschiffahrt, Vol. 12, p. 273, Sept. 30, 1921.

Reference 3. Reissner, H.: Die Seitensteuerung der Flugmaschinen. Zeitschrift für Flugtechnik und Motorluftschiffahrt, Vol. 1, pp. 101 and 117, May 10 and 28, 1910.

Reference 4. Gates, S. B., and Bryant, L. W.: The Spinning of Aeroplanes. British A.R.C. R&M No. 1001, 1926.

Reference 5. Glauert, H.: The Investigation of the Spin of an Aeroplane. British A.C.A. R&M No. 618, 1919.

Reference 6. Irving, H. B., Batson, A. S., Frazer, R. A., and Gadd, A. G.: Experiments on a Model of a Bristol Fighter Aeroplane (1/10th scale).
Part I: Force and Moment Measurements at Various Angles of Yaw. By H. B. Irving and A. S. Batson.
Part II: Lateral Derivatives by the Forced Oscillation Method. By R. A. Frazer, A. S. Batson, and A. G. Gadd.
British A.R.C. R&M No. 932, 1924.

References and Bibliography (Contd.)

Reference 7. Irving, H. B., Batson, A. S., Townend, H. C. H., and Kirkup, T. A.: Some Experiments on a Model of a B.A.T. Bantam Aeroplane with Special Reference to Spinning Accidents.
Part I: Longitudinal Control and Rolling Experiments. By H. B. Irving and A. S. Batson.
Part II: Experiments on Forces and Moments (Including Rudder Control). By H. C. H. Townend and T. A. Kirkup.
British A.R.C. R&M No. 976, 1925.

Reference 8. Bradfield, F. B.: Lateral Control of Bristol Fighter at Low Speeds. Measurement of Rolling and Yawing Moments of Model Wings Due to Rolling. British A.R.C. R&M No. 787, 1921.

Reference 9. Irving, H. B., and Batson, A. S.: Preliminary Note on the Effect of Stagger and Decalage on the Auto-Rotation of a R.A.F. 15 Biplane. British A.R.C. R&M No. 733, 1920.

Korvin-Kroukowsky, B. V.: Tail Spins and Flat Spins. Aviation, July 18, 1927.

Translation by J. Vanier,
National Advisory Committee
for Aeronautics.

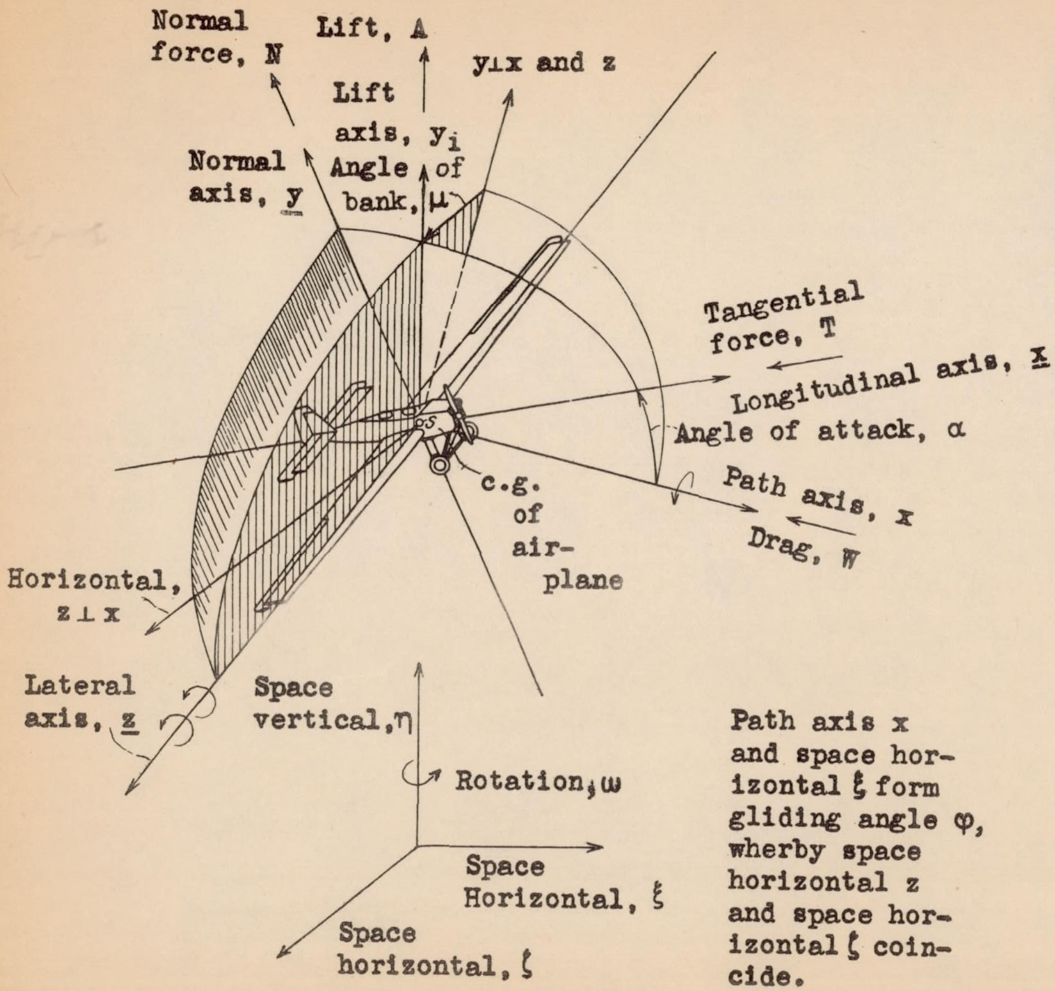

Path axis x and space horizontal ξ form gliding angle φ, wherby space horizontal z and space horizontal ζ coincide.

Fig.1
Direction of axes, angles and forces.

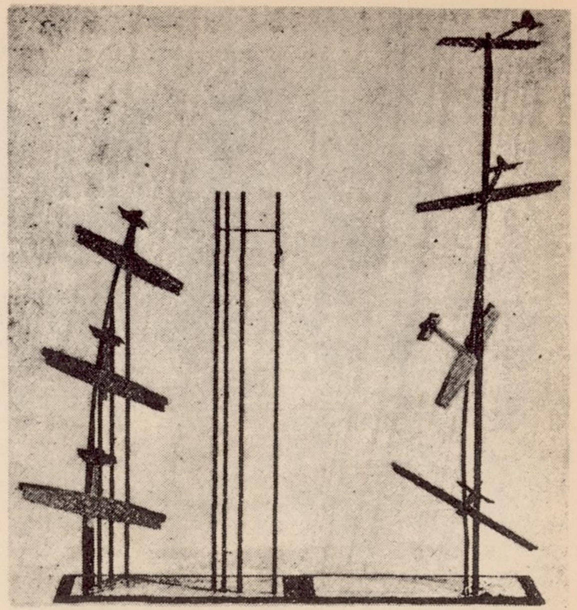

Fig. 37
Models illustrating the effect of an elevator displacement in steep and flat spin. The vertical bars, not relating to the path, denote the incidental spinning axes.

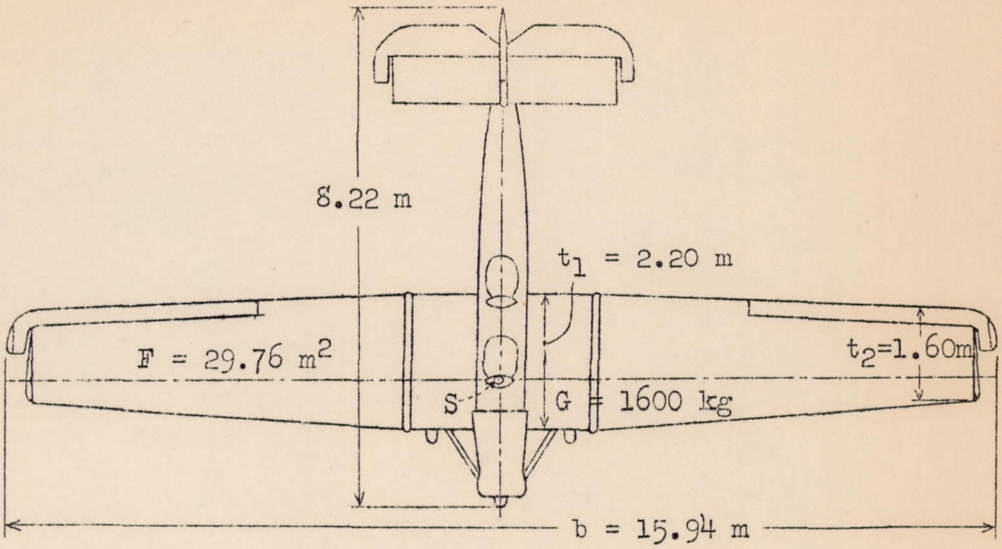

Fig.2

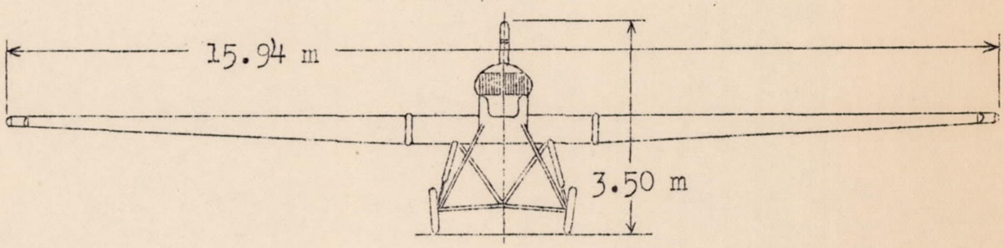

Fig.3

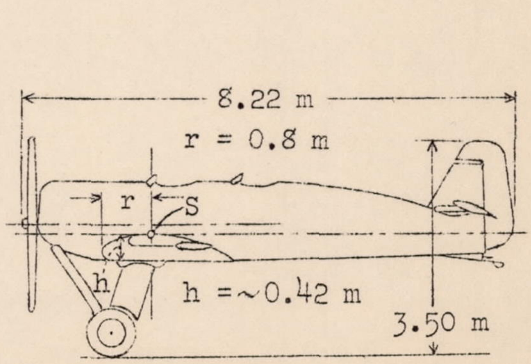

Fig.4

Figs.2,3,4 Three view drawing of Junkers A35 model airplane.

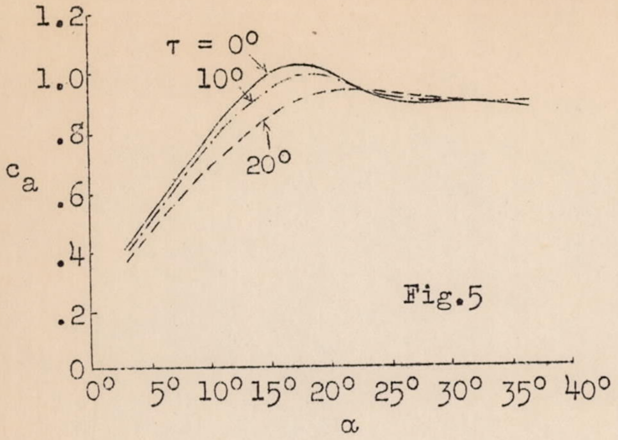

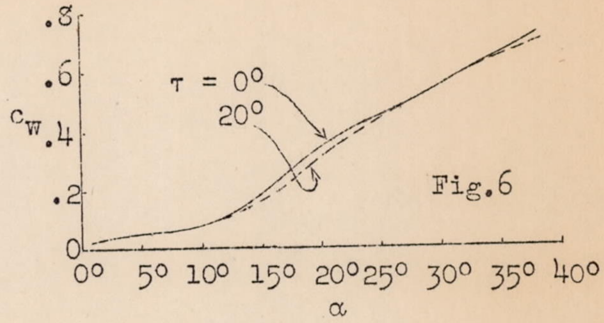

Figs.5,6 Lift and drag plotted against α and φ. (Reference 6)

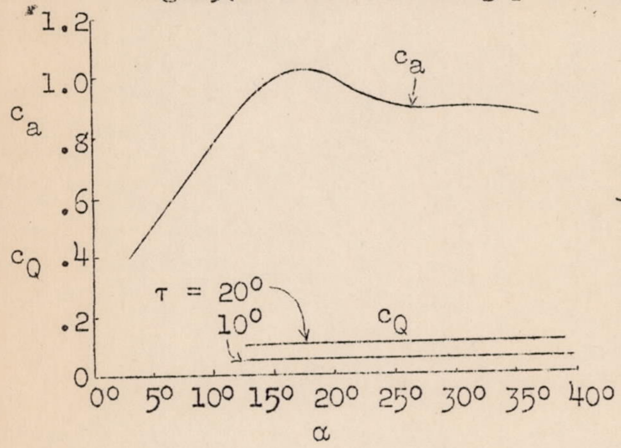

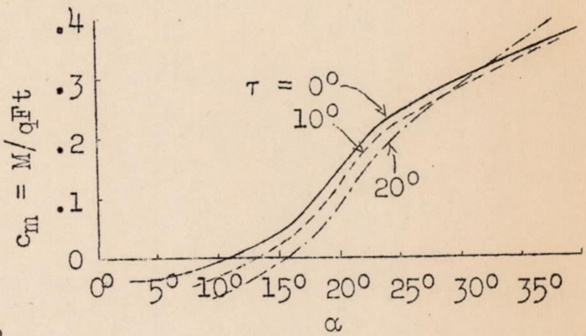

Fig.8 Aerodynamic moment about lateral axis against α and τ. (Reference 7)

Fig.7 Cross wind force due to sideslip plotted against α and in comparison to lift with no sideslip (Reference 6)

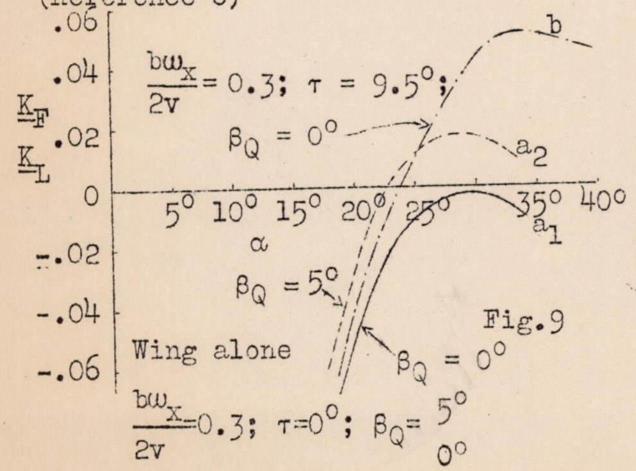

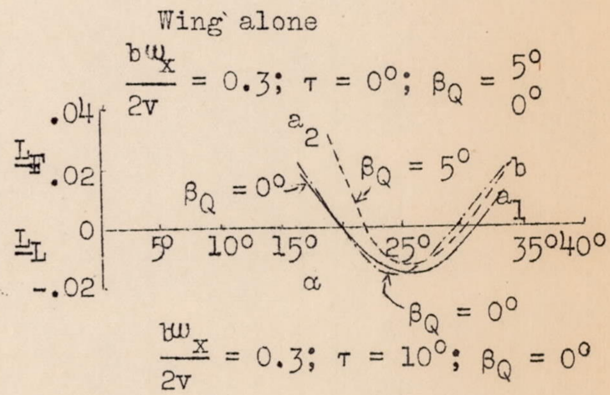

Fig.10

Figs.9,10 Aerodynamic moment about longitudinal and normal axis plotted against α and τ, as well as against ω_x about path axis and aileron displacement β_Q, (Reference 8 and 4).

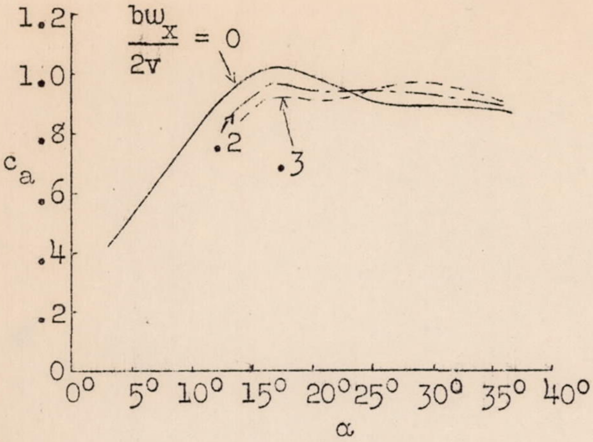

Fig.11

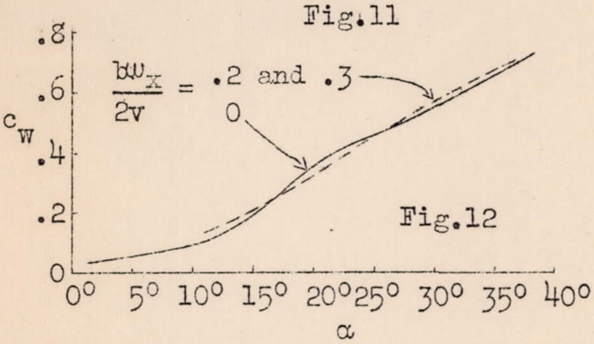

Fig.12

Figs.11,12 Lift and drag against α and rotation ω_x about path axis (Reference 4).

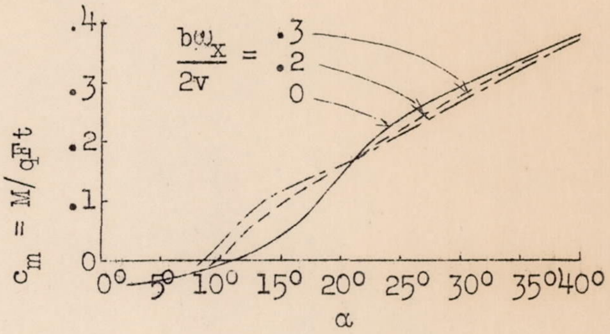

Fig.13 Aerodynamic moment about lateral axis against α and against rotation ω_x about path axis (Reference 7).

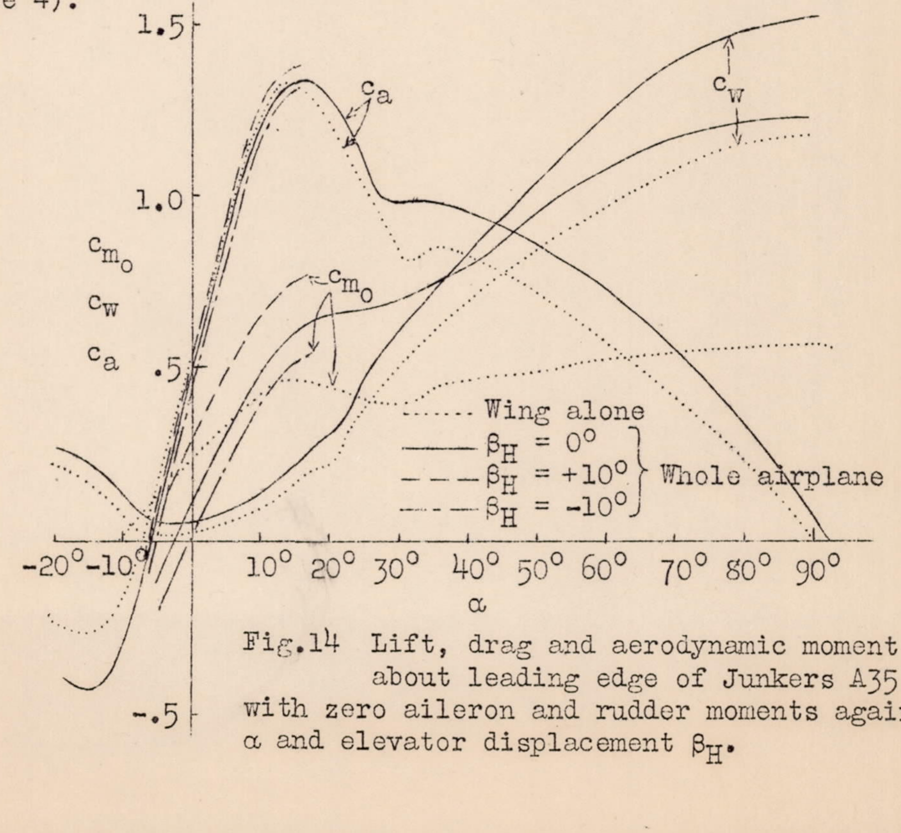

Fig.14 Lift, drag and aerodynamic moment about leading edge of Junkers A35 with zero aileron and rudder moments against α and elevator displacement β_H.

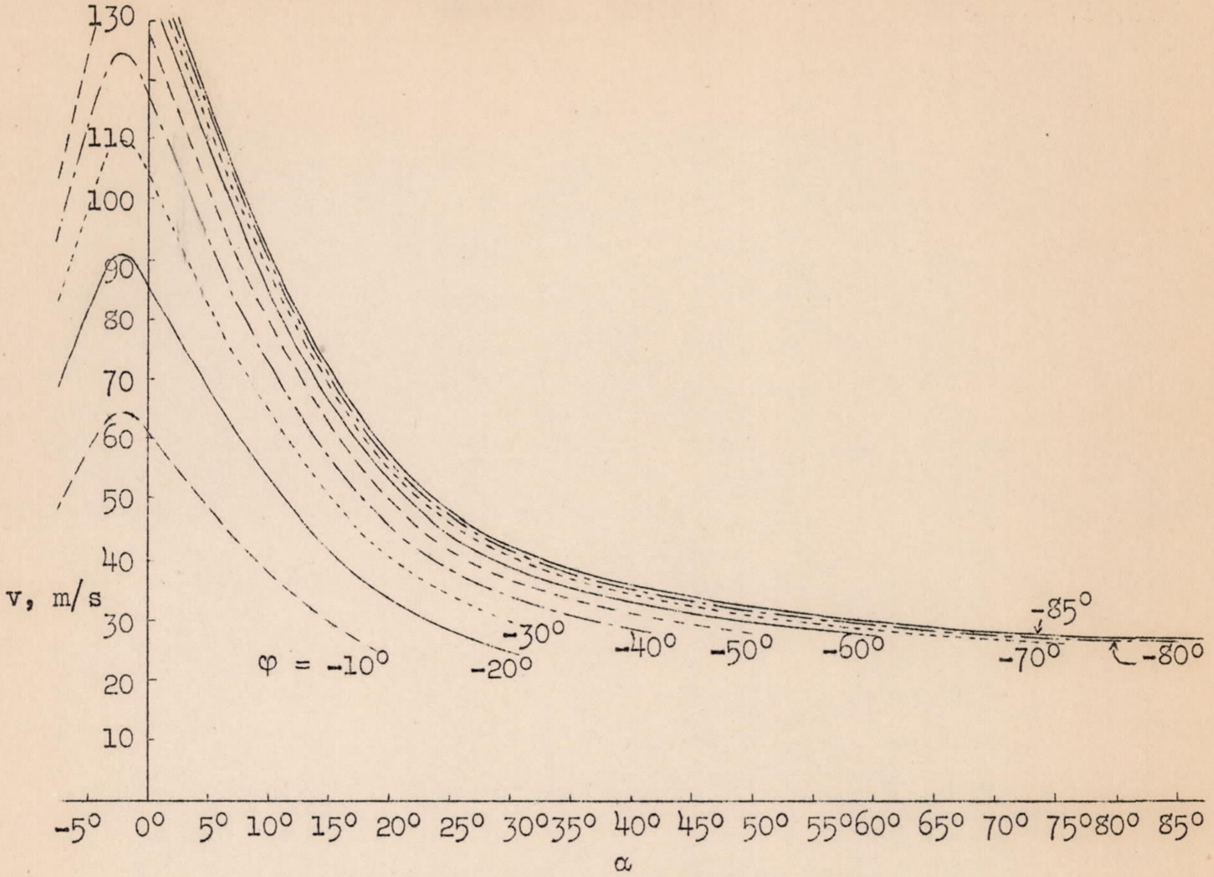

Fig.15 Path velocity against α and φ.

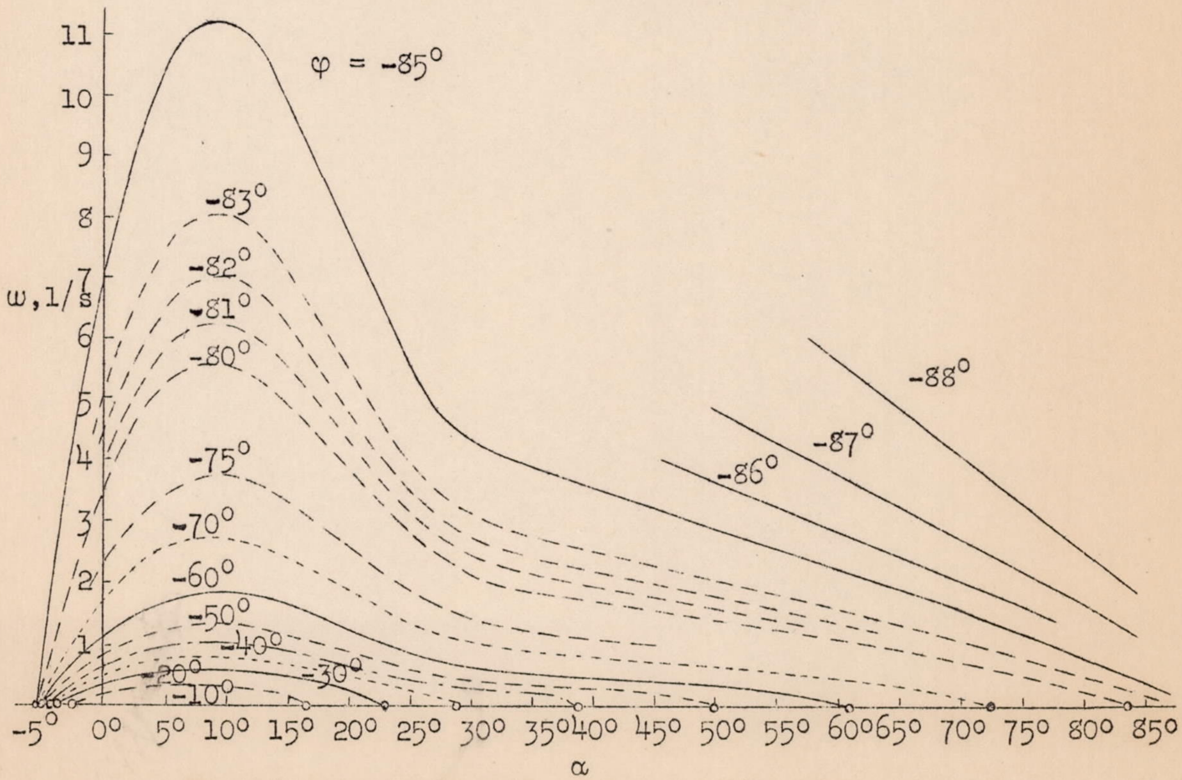

Fig.16 Rate of rotation against α and φ.

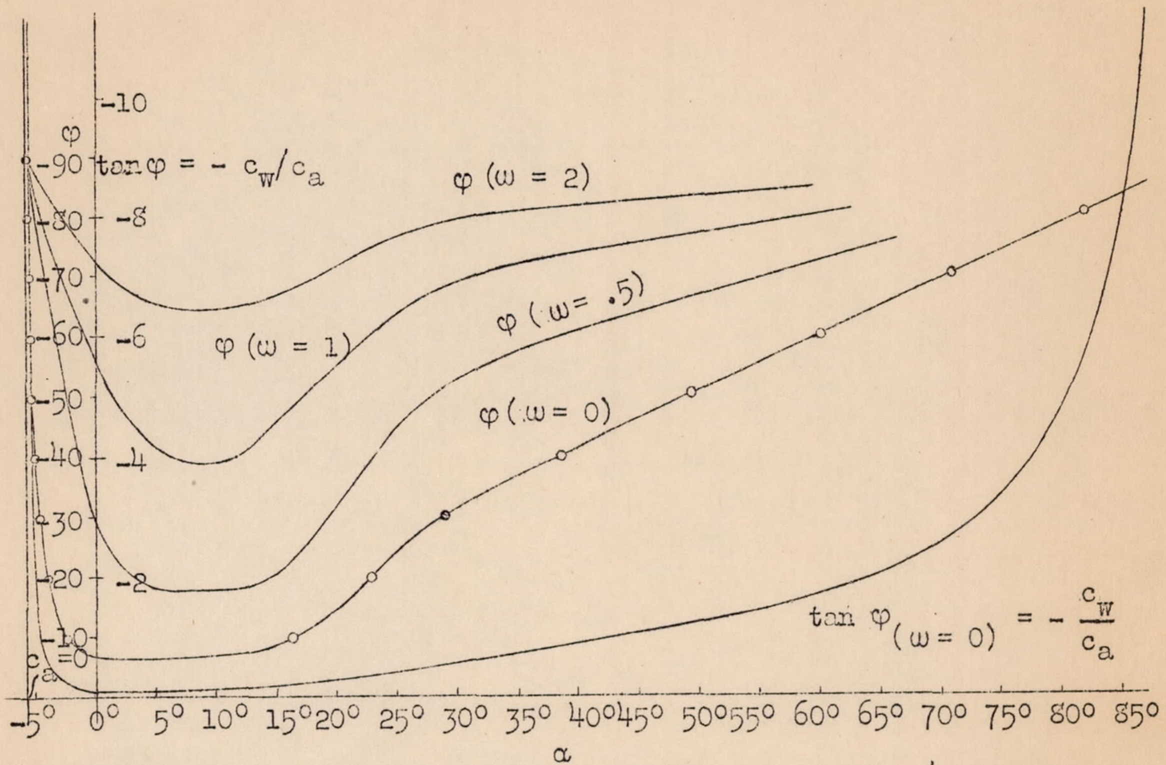

Fig.17 Angle of glide $\varphi_{(\omega = \text{const.})}$ and $\tan\varphi_{(\omega = 0)} = - c_a/c_w$ against α and rate of rotation.

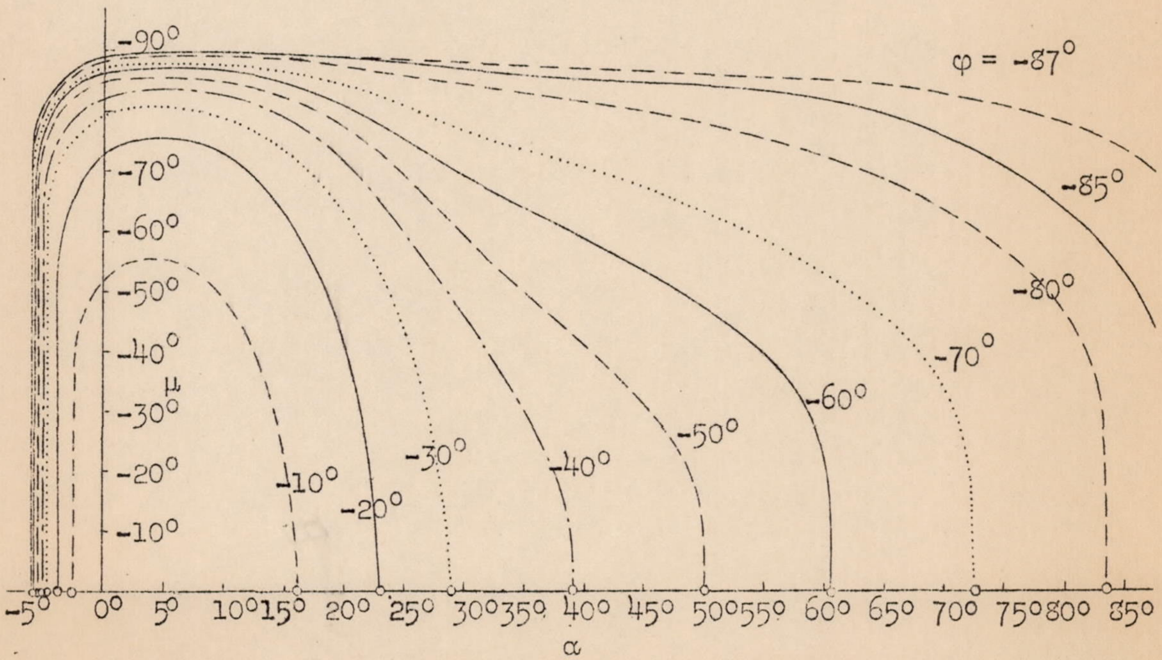

Fig.18 Angle of bank against α and φ.

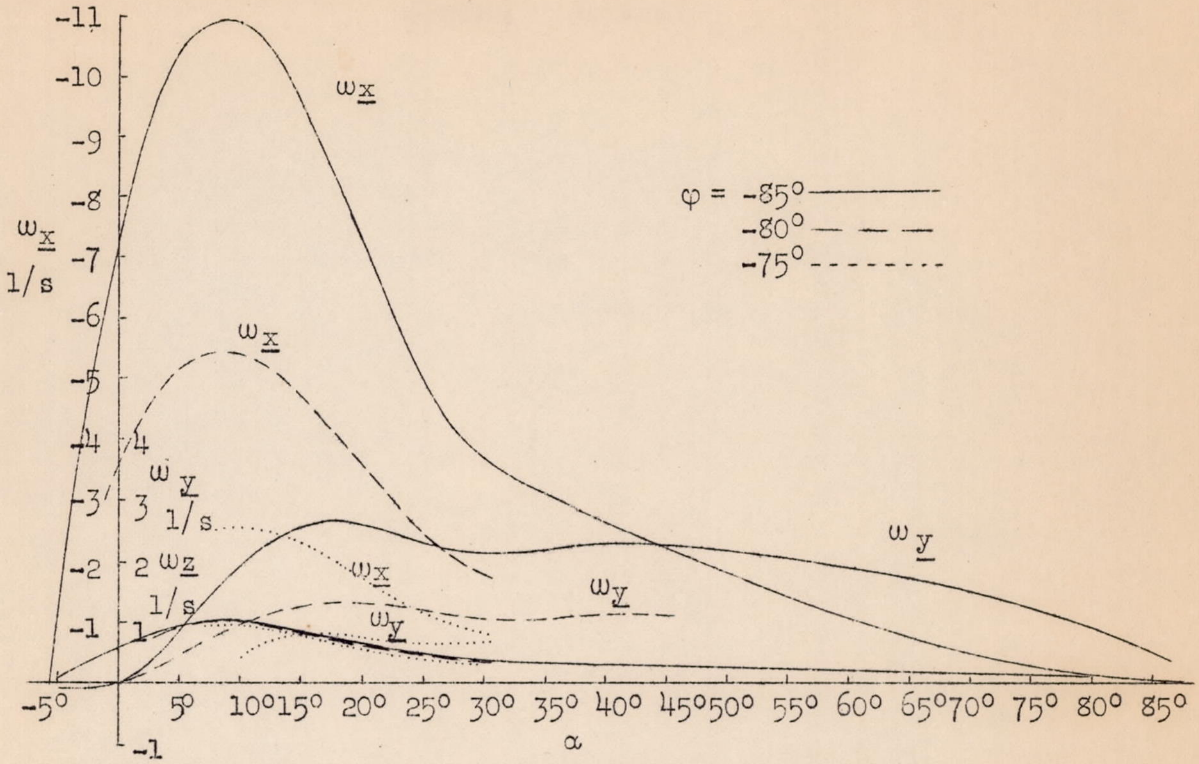

Fig.19 Rate of rotation about the body axes against α and φ .

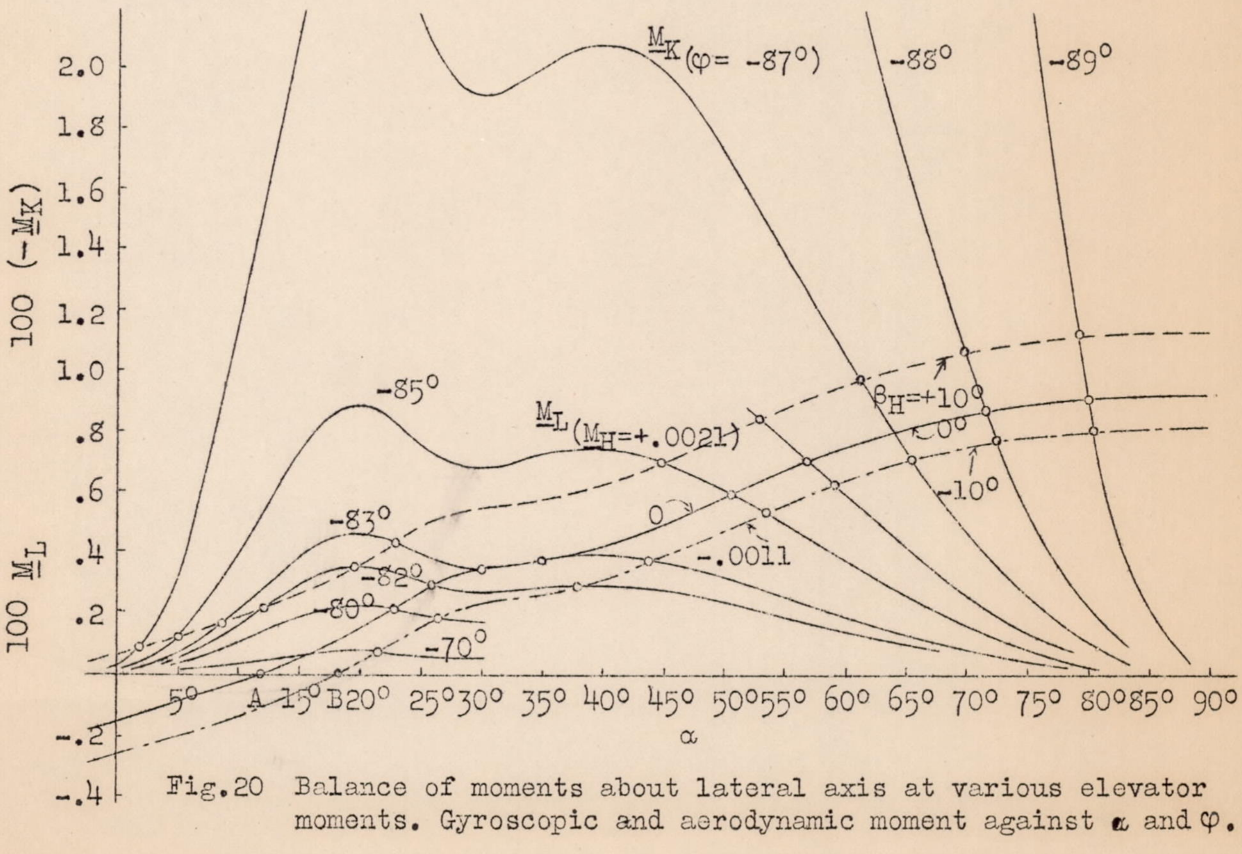

Fig.20 Balance of moments about lateral axis at various elevator moments. Gyroscopic and aerodynamic moment against α and φ.

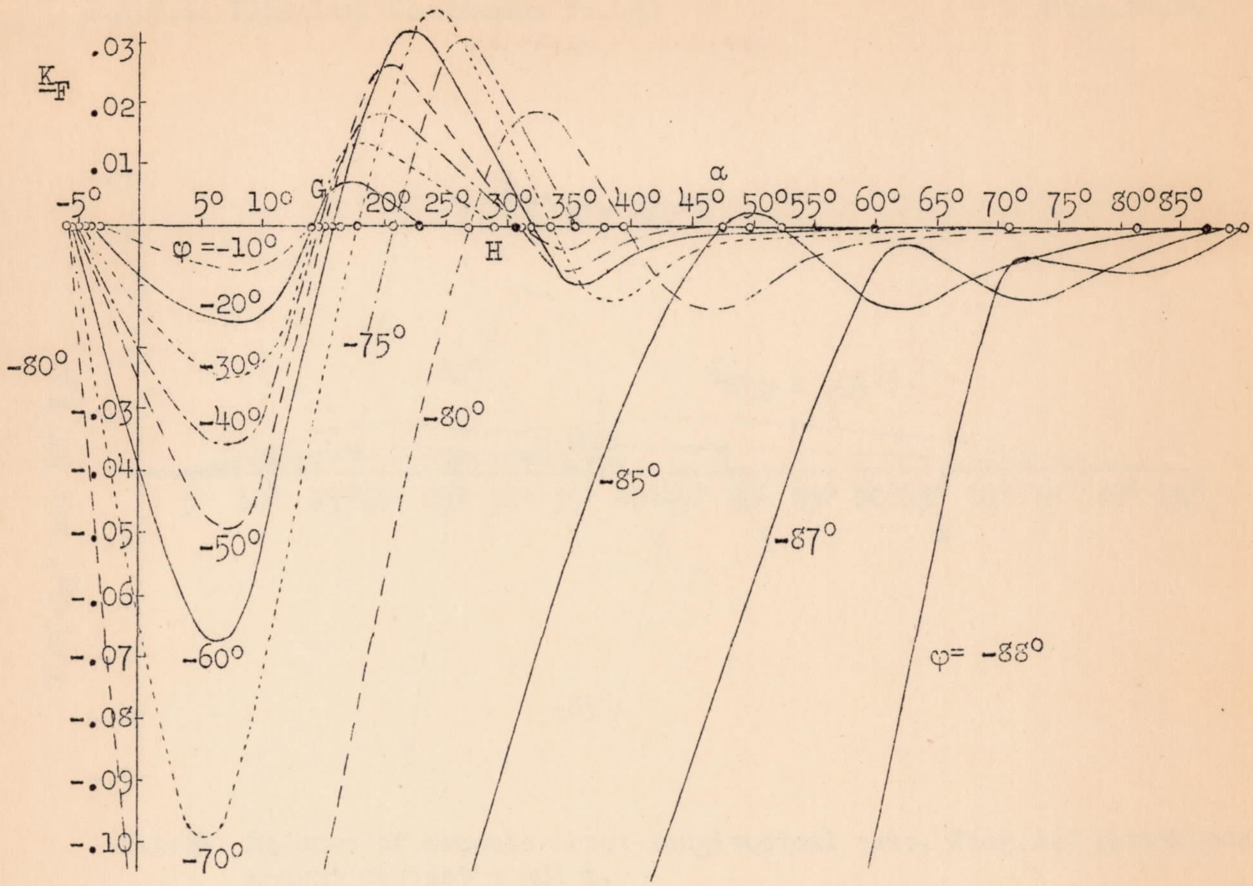

Fig.22 Balance of moments about longitudinal axis. Aerodynamic moment of wing against α and φ.

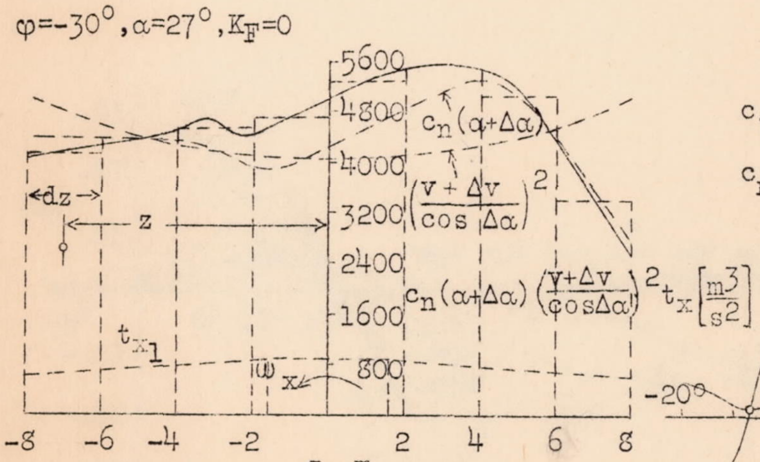

Fig.21 Distribution of normal force across the wing.

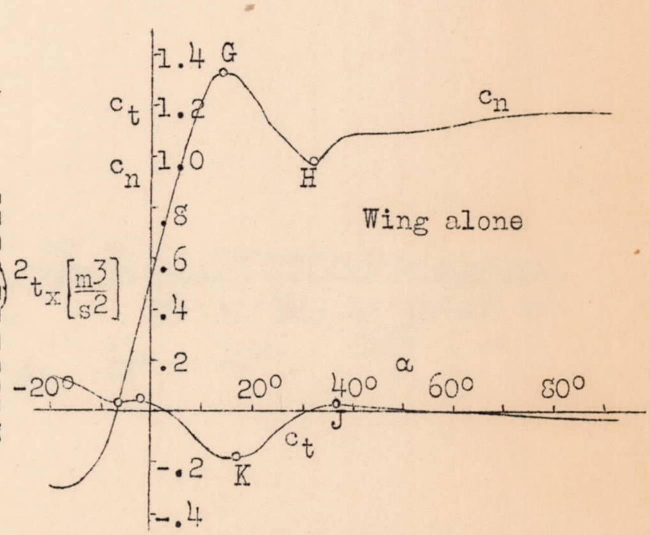

Fig.23 Normal and tangential force of wing alone against α.

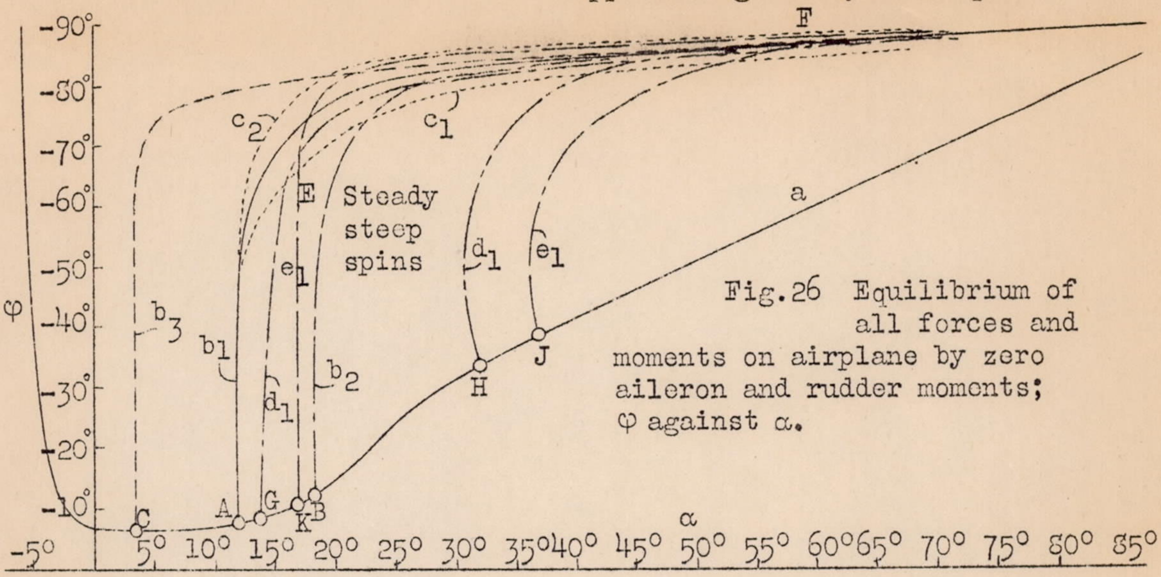

Fig.26 Equilibrium of all forces and moments on airplane by zero aileron and rudder moments; φ against α.

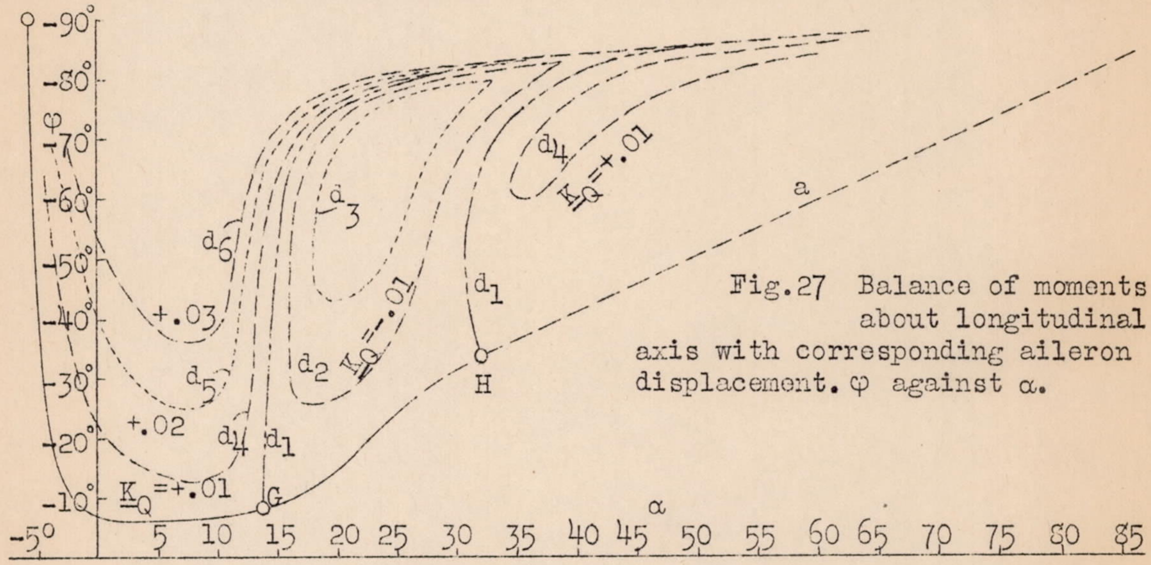

Fig.27 Balance of moments about longitudinal axis with corresponding aileron displacement. φ against α.

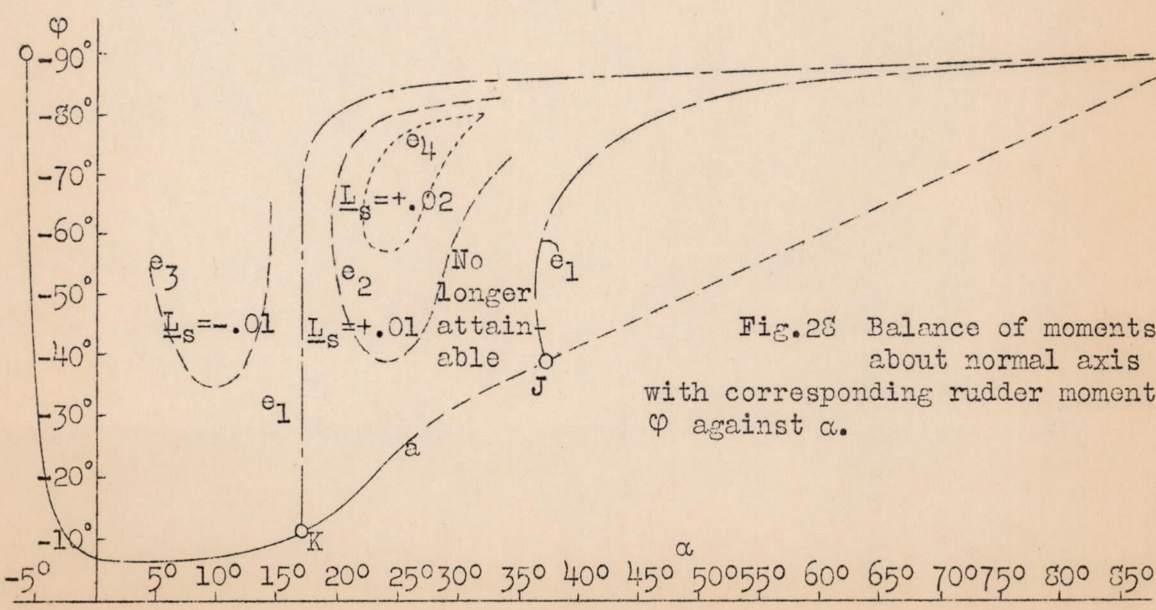

Fig.28 Balance of moments about normal axis with corresponding rudder moments. φ against α.

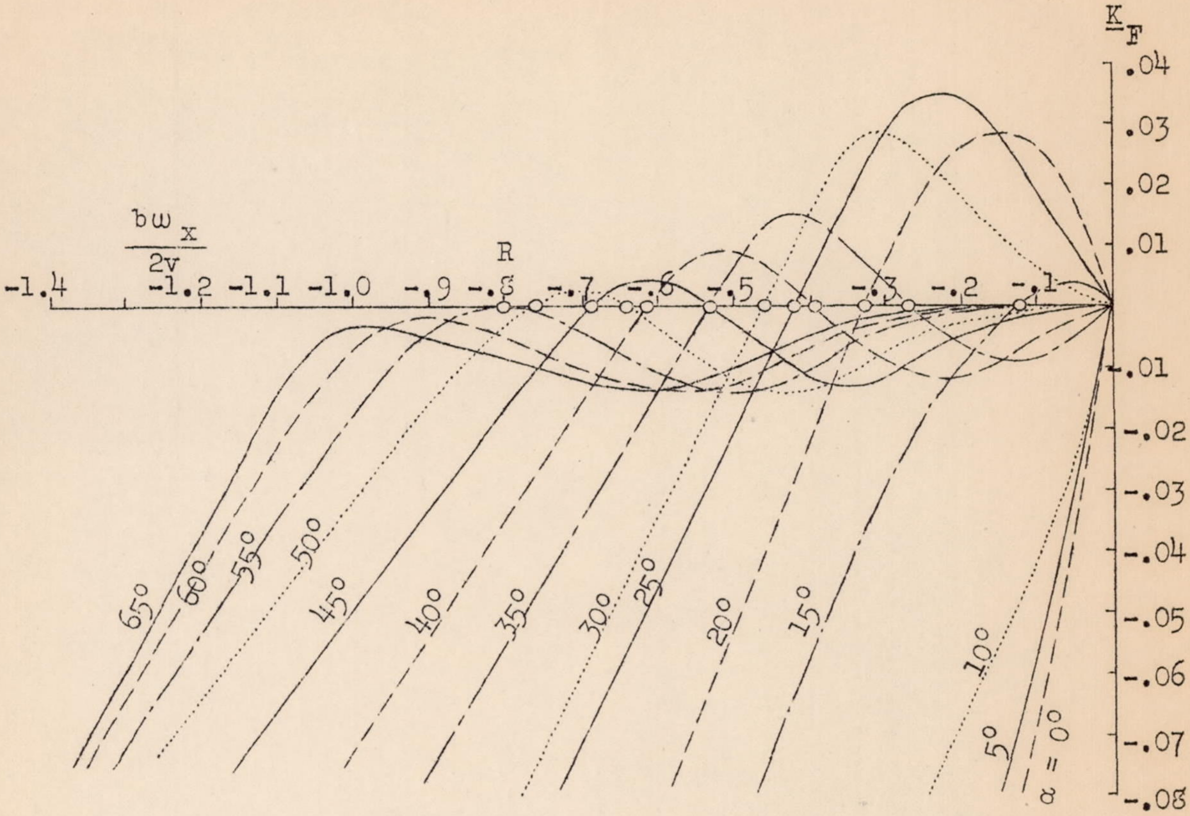

Fig.29 Wing moment about longitudinal axis against α and $\frac{b\omega_x}{2v}$.

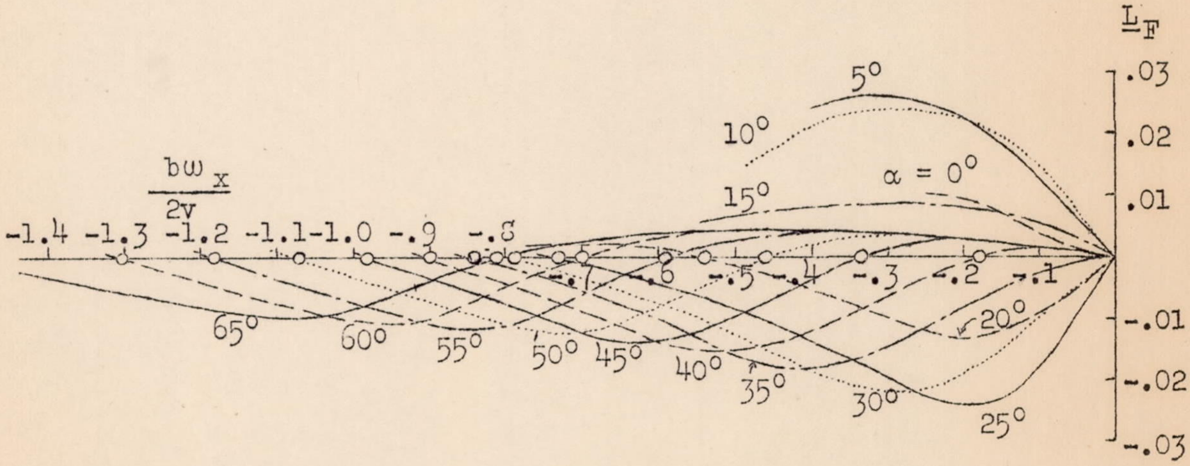

Fig.30 Wing moment about normal axis against α and $\frac{b\omega_x}{2v}$.

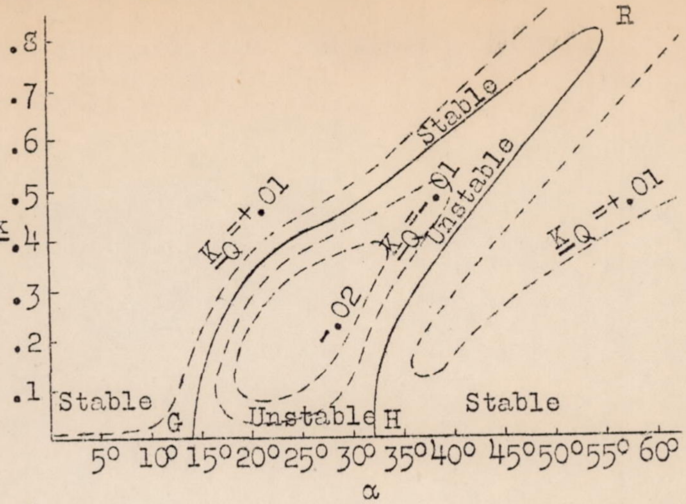

Fig.31 Balance of moments about longitudinal axis for various aileron moments $\frac{b\omega_x}{2v}$ plotted against α.

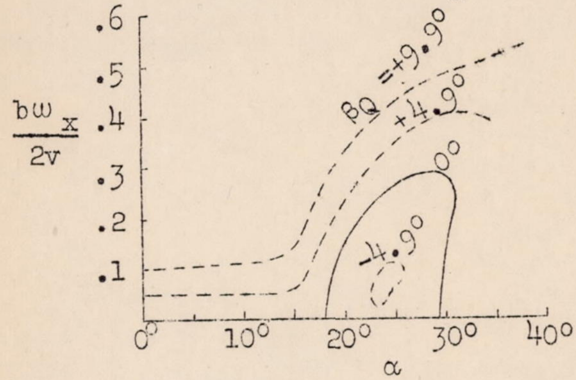

Fig.32 Balance of moments about path axis of a wing; $\frac{b\omega_x}{2v}$ plotted against α and β_Q.

(Reference 8)

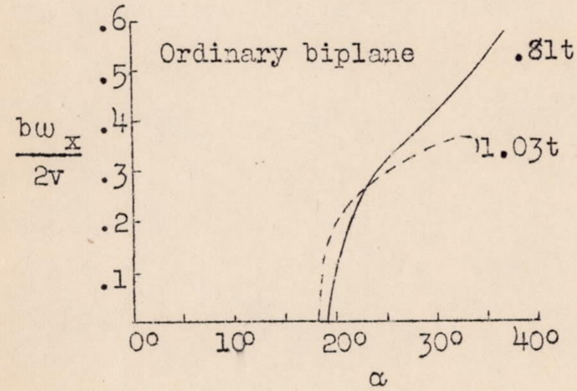

Fig.33 Balance of moments about path axis of a biplane; $\frac{b\omega_x}{2v}$ plotted against α and wing gap. (Reference 7)

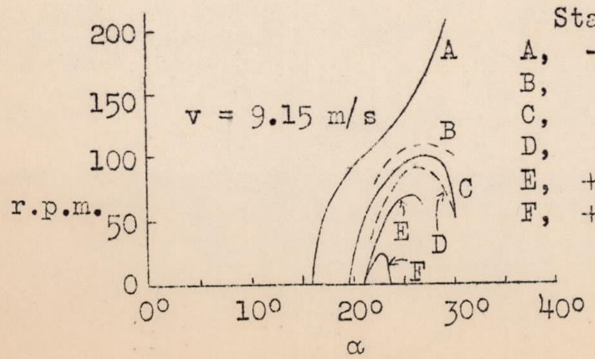

	Stagger	Decalage
A,	-25°	0°
B,	0°	-2°
C,	0°	0°
D,	0°	+2°
E,	+25°	-1°
F,	+25°	-2°

Fig.34 Balance of moments about path axis of a biplane; rate of rotation about path axis plotted against α, stagger and decalage. (Reference 9)

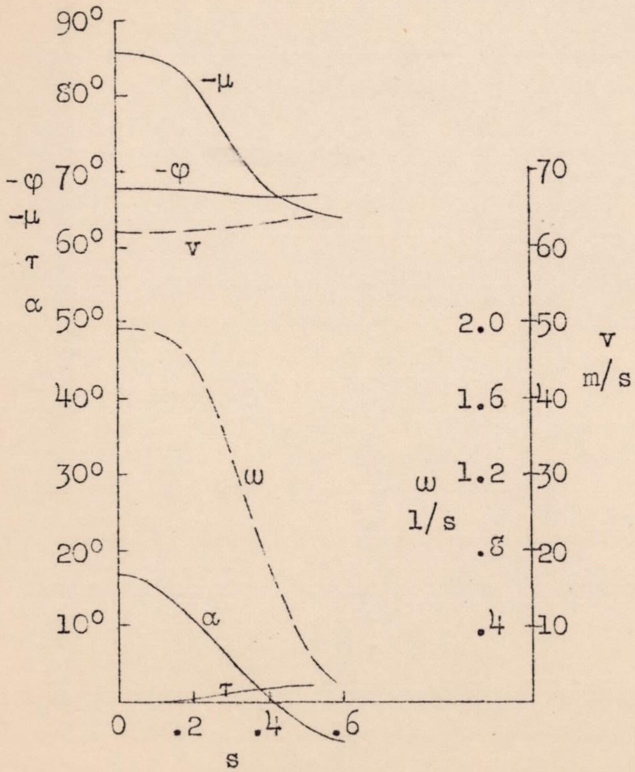

Fig.35

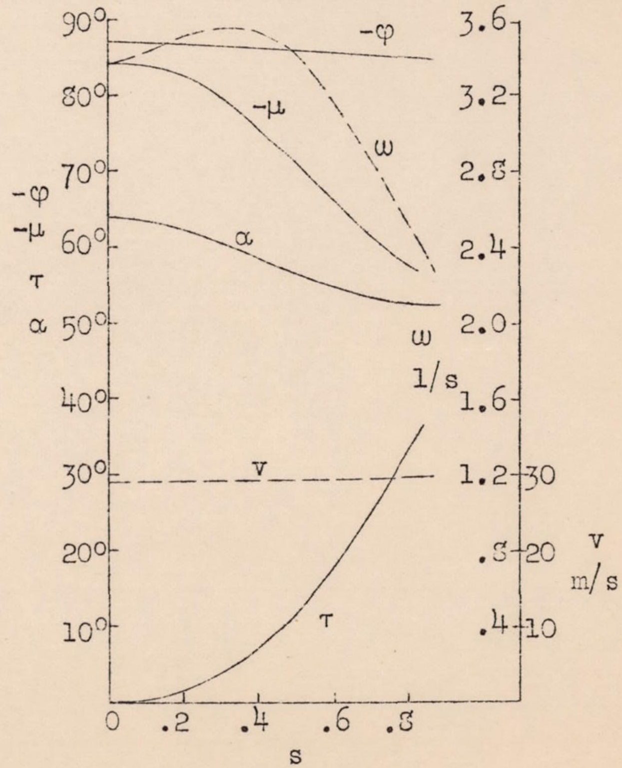

Fig,36

Figs.35,36 Change in flight attitude due to an elevator moment $\underline{M}_H = +0.0021$ (displacement downward) in a not dangerous steep and a dangerous flat spin for zero aileron, and rudder moment. The 5 variables are referable to time.